Journal of Power Sources 193 (2009) 249–257

Contents lists available at ScienceDirect

Journal of Power Sources

journal homepage: www.elsevier.com/locate/jpowsour

Water management in a single cell proton exchange membrane fuel cells with a serpentine flow field

Nik Suhaimi Mat Hassan, Wan Ramli Wan Daud*, Kamaruzzaman Sopian, Jaafar Sahari

Fuel Cell Institute, Universiti Kebangsaan Malaysia, 43600 Bangi, Selangor, Malaysia

ARTICLE INFO

Article history:
Received 28 October 2008
Received in revised form 14 January 2009
Accepted 15 January 2009
Available online 5 February 2009

Keywords:
Water management
PEMFC
Moisture profile
Mass transfer coefficient
Diffusivity

ABSTRACT

Gas and water management is the key to achieving good performance from a polymer electrolyte membrane fuel cell (PEMFC) stack. Imbalance between production and evaporation rates can result in either flooding of the electrodes or membrane dehydration, both of which severely limit fuel cell performance. In the present study, a mathematical model was developed to evaluate moisture profiles of hydrogen and air flows in the flow field channels of both the anode and the cathode. For model validation, a single fuel cell was designed with an active area of 200 cm^2. Six humidity sensors were installed in the flow fields of both the anode and the cathode at 457 mm, 1266 mm and 2532 mm from the inlets. The experiment was performed using an Arbin Fuel Cell Test Station. The temperature was varied (25 °C, 40 °C, 50 °C and 60 °C), while hydrogen and air velocities were fixed at 3 L min^{-1} and 6 L min^{-1}, respectively, during the operation of the single cell. The feed relative humidity at the anode was fixed at 1.0, while the feed relative humidity at the cathode was fixed at 0.005 (dry air). All humidity sensor readings were taken at steady state after 2 h of operation. Model predictions were then compared with experimental results by using the least squares algorithm. The moisture content was found to decrease along the flow field at the anode, but to increase at the cathode. The moisture content profile at the anode was shown to depend on the moisture Peclet number, which decreased with temperature. On the other hand, the moisture profile at the cathode was shown to depend on both the Peclet number and the Damkohler number. The trend of the Peclet number in the cathode followed closely that of the anode. The Damkohler number decreased with temperature, indicating increasing moisture mass transfer with temperature. The moisture profile models were successfully validated by the published data of the estimated overall mass transfer coefficient and moisture effective diffusivity of the same order of magnitude. The strategy of saturating the hydrogen feed and using dry air, as in the present work, has been shown to successfully prevent water droplet formation in the cathode, and hence prevent flooding.

1. Introduction

Water plays a critical role in PEM fuel cells (PEMFC). Good PEMFC performance depends on good water management. Extra humidification of the reactant gases is essential in PEMFC operating above 60 °C because water vapour is continuously lost in the exhaust gases, and membranes must be hydrated to better conduct protons [1]. If the membrane is not properly hydrated, its ionic resistance increases, and in extreme cases, it can be completely destroyed. The methods normally used to keep the membrane hydrated are internal and external humidification. In "self-humidifying" internal humidification, a catalyst in the membrane electrode assembly (MEA) is modified to not only to retain, but also to produce water [2]. This process is passive and most suitable for small cells. In contrast, in the external humidification method, the fuel gas and air are passed through water columns of separate humidifier bottles until they are fully saturated before entering the fuel cell stack [3]. The humidifier bottle temperatures are controlled independently from the stack temperature to get the desired gas temperature and relative humidity. The external humidification method is widely used in small scale laboratory fuel cell experiments as well as in larger pilot plant scale fuel cell systems due to its simplicity. This laboratory has investigated the humidification load of a similar external humidifier [4]. In the present work, a fuel cell operating technique was developed to manage water in the fuel cell by maintaining a moisture gradient across the membrane from the anode to the cathode. The effectiveness of the technique was investigated via modelling and measuring the variation of humidity in the air and hydrogen along the flow fields of both electrodes in a single cell fuel cell.

* Corresponding author. Tel.: +60 3 89217078; fax: +60 3 89216024.
E-mail address: wramli@eng.ukm.my (W.R.W. Daud).

0378-7753/$ – see front matter © 2009 Elsevier B.V. All rights reserved.
doi:10.1016/j.jpowsour.2009.01.066

Nomenclature

a_S	specific surface area of the electrode ($m^2\ m^{-3}$)
b	flow channel depth (m)
$C_{O_2}^{ref}$	reference molar concentration of oxygen ($mol\ m^{-3}$)
d_p	pore diameter (m)
Da	Damkohler number (–)
D_{eff}	diffusivity ($m\ s^{-1}$)
D_{O_2}	diffusion coefficient of the dissolved oxygen in the electrolyte ($mol\ cm^{-1}\ s^{-1}$)
F	Faraday's constant ($A\ s\ mol^{-1}$)
G	coefficient
H	Henry's constant ($Pa\ m^3\ mol^{-1}$)
i_O	exchange current density ($mA\ cm^{-3}$)
i_{OC}	exchange current density in the cathodic active layer ($mA\ cm^{-2}$)
J_A	moisture condensation flux on the surface of the anode ($mol\ cm^{-2}\ s^{-1}$)
J_C	moisture evaporation flux on the surface of the cathode ($mol\ cm^{-2}\ s^{-1}$)
J_w	moisture flux across the membrane ($mol\ cm^{-2}\ s^{-1}$)
k_A	moisture mass transfer coefficient at the anode ($mol\ cm^{-2}\ s^{-1}$)
K	K-value of moisture
K_4	constant
K_5	constant
K_6	constant
k_C	moisture mass transfer coefficient at the cathode ($mol\ cm^{-2}\ s^{-1}$)
k_g	overall moisture mass transfer coefficient ($mol\ cm^{-2}\ s^{-1}$)
L	total length of the flow field (m)
m	evaporation index (–)
M	coefficient (–)
n	evaporation index (–)
p	total pressure (Pa)
p_{sat}	saturated vapour pressure of moisture (Pa)
Q	coefficient
Pe	Peclet number (–)
r	rate of water production by the electrochemical reaction ($mol\ s^{-1}$)
R	gas constant ($J\ mol^{-1}\ K^{-1}$)
t_e	active layer thickness (m)
T	temperature (K)
v	gas velocity ($m\ s^{-1}$)
w	channel width (m)
x_A^*	equilibrium moisture content of membrane
x_{Ci}	molar moisture content at the surface of cathode
y_A	molar moisture content at the anode
y_A^*	equilibrium moisture content at membrane surface
y_{AF}	hydrogen feed moisture content
y_C	molar moisture content at the cathode
y_{CF}	air feed moisture content
y_{Ci}	molar moisture content of gas at the surface of cathode
z	distance along flow field (m)
z^*	dimensionless distance

Greek letters

ε	dry porosity of the electrode
ϕ	relative humidity
$\Delta\varphi_{eq}$	potential difference between the electrode and the membrane (V)
φ_s, φ_m	electrode and membrane potential (V)

2. Water transport in PEMFC

Membrane hydration is affected by water transport in the membrane itself, which, in turn, is affected by the condition of the inlet gases and the operating parameters of the fuel cell. Water is transported through the membrane in three ways: electro-osmotic drag by protons from the anode to the cathode, back diffusion due to concentration gradients from the cathode to the anode (or vice versa in limited cases), and convective transfer due to pressure gradients within the stack.

Current research has focused on both the electro-osmotic drag and the back diffusion as the dominant mechanisms for water transport within the membrane. Both water transport mechanisms are functions of the fuel cell temperature, current density and membrane water content. In electro-osmotic drag, protons that move from the anode to the cathode drag water molecules with them. The number of water molecules carried by each proton is normally between 0.5 and 1.5 molecules per proton [5]. As a result, the moisture content in the hydrogen decreases along the flow channel. As more current is drawn from the fuel cell, the flow of protons and water from the anode to the cathode increases. However, at the same time, water that is being produced at the cathode by the oxygen reduction reaction begins to diffuse back through the membrane to the anode. The key to understanding membrane hydration is the balance that has to be struck between the electro-osmotic drag and back diffusion [5].

At high current density, the membrane dries out because water transport from the anode by electro-osmotic drag exceeds its transport to the anode by back diffusion from the cathode [6]. The pores of the dry membrane also shrink, thus further limiting the back diffusion of water. Water transport due to back diffusion is not sufficient to prevent membrane dehydration [6,7]. The net water flux from the anode to the cathode is directly proportional to the current density [7,8]. At high current densities, the large electro-osmotic drag from the anode dries out the anode and floods the cathode [7,8]. The reduction reaction at the cathode is adversely affected by the increase in water content at the cathode [8].

Cell voltage can also be reduced when membrane moisture content is low due to anode dehydration [5]. High cell voltage can be achieved by saturating the inlet hydrogen with water to increase the water flux from the cathode to the anode [5]. Dry hydrogen carries away three and a half times more water molecules from the anode than does the air from the cathode [9]. If both inlet gases are humidified, the water profile in the membrane electrolyte is uniform, the resistance of the membrane remains low, and higher cell voltages can be achieved. However, the saturated air at the cathode may prevent evaporation of the water produced by the oxidation reaction and cause flooding, which reduces the cell voltage.

Recent works on water management have shifted their focus of managing water in PEMFC from water transport in the MEA to water transport in the gases, which can be controlled by manipulating operating variables of the PEMFC stack such as the temperature, humidity and pressure of the gases. The understanding of the roles of these variables on water management is still rudimentary. This is reflected in the use of either dry gases or fully humidified saturated gases [10–12]. The water content of the gases in the PEMFC cell was previously found to affect current density distribution on the electrode and therefore the PEMFC performance [13]. It has also been suggested that effective water management could be achieved by controlling water content in the feed gases [10]. However, the low current density and performance of the PEMFC were attributed to low proton transport caused by the dryer polymer electrolyte membrane, which in turn was caused by the dryer air [10–12]. The conventional solution for maintaining a sufficiently wet membrane for maximum proton transport is to use fully humidified saturated hydrogen and air. However, this solution complicates the balance of

plant design and operation and often leads to flooding because liquid water will always condense in the air at the saturated condition approaching water dew point.

The main challenge in doing this is maintaining a sufficiently wet membrane for maximum proton transport without flooding the PEMFC. Flooding occurs when the wet gas in the PEMFC reaches its dew point [13] or, in other words, its saturation point. Humidifying both gases fully to saturation will certainly lead to flooding. In the present work, an alternative operating technique for better water management by manipulating the water content and temperature of the feed gases is proposed. Water produced at the cathode is removed as soon as it is formed through evaporation by the dryer air to avoid flooding at the cathode, which may cause the MEA to become dry. If a fully humidified and saturated hydrogen is used at the anode and a partially humidified air is used at the cathode, the water flux is forced to flow from the anode to the cathode because of the difference of humidity in the hydrogen and air feed. In this manner, the water content in the membrane can be maintained and flooding avoided.

3. Modelling of water profile in the PEMFC

A clearer understanding of water transport in a PEM fuel cell can be obtained by validating water transport models with experimental data. Many models developed to explain water transport in PEM fuel cells in the past were either based on water flow dominated by transport in the MEA or in the gas flow channels.

Early one dimensional models considered water flow across the membrane in the MEA either as a function of the hydraulic pressure gradient and the electro-osmotic drag in a uniformly wetted membrane with porous two phase catalyst layers [14] or as a function of the electro-osmotic drag and the diffusion of water down a moisture content gradient across the electrolyte membrane [5]. The MEA centred models were varied by replacing the homogenous two phase model of catalyst layer by an agglomerate model [15] and by combining the electrolyte membrane model and the agglomerate catalyst layer model in a single MEA [16]. When liquid water flooding became a major problem in PEM fuel cells operation, the catalyst layer model was modified by having liquid water and polymer electrolyte in its pores [17]. The reactant gases were also included in the pores when it became clear that two phase flow may have occurred in the catalyst layer [18] and in the electrode backing [19]. The MEA centered model was further varied by incorporating a one dimensional single phase flow model of reactant gas in the flow channels and heat transfer between the bipolar plate, cooling water, reactant gas and MEA [6,7,15]. This was followed by the development of two [20,21] and three dimensional MEA models [22].

With the advent of computational fluid dynamic modelling (CFD) and its success in modelling complex fluid flow problems in engineering at the turn of the new millennium, water transport in the gas flow channels was modelled extensively using CFD with the water and the energy fluxes at the MEA surfaces treated as simple source terms at the boundary [23–27]. The CFD model was further extended by replacing the boundary water source with Henry's Law where the water content in the gas phase is a function of the moisture content in the electrolyte [28] and by considering the existence of two phase flow in the gas channels [29–31].

At almost the same time, a more unified approach to PEM fuel cells model emerged where the electrolyte, the catalyst layer and backing, and the gas flow channel were rigorously modelled. The water and ion transport models in the MEA were either based on the earlier MEA dominated models [32] or the more rigorous Stefan–Maxwell multi-component diffusion model [33,34]. Water transport in the gas channel was in the gas phase only while that in the porous catalyst layer was thought to occur in two homogenous phases [18,32,34] or in multiphase mixtures [35–38]. The water transport in the gas channel and the MEA were coupled by using either Henry's Law [37] and Newton's Law of cooling [39] to generate the interfacial water source or using interfacial water flux from the water transport equations in the electrolyte and catalyst layers, and in the gas flowing in the channels [40]. The unified model was further improved by incorporating two phase water transport in the channels [41–44].

A less known but equally important PEM fuel cells model, the lumped or stirred tank reactor model, where the fuel cell is regarded as a black box and the fuel cell reaction is assumed uniform throughout the fuel cell without any spatial variation, was principally used in modelling the dynamic response and control of PEM fuel cells [45–49]. Its use for water management is limited because it could not show the spatial variation of water content in the PEM fuel cells. However, if the single stirred tank reactor or lumped model were extended to multiple lumps or stirred tank reactors where the fuel cell is divided into multiple stirred tanks in series along the flow field, then water content variation along the channel could be determined easily and the accuracy of prediction could be adjusted by the number of tanks used [50–52].

In this paper, a model for the water content profiles along the flow channels at both the anode and the cathode was developed in order to understand the water flow in the PEM fuel cell. The new model assumes that the PEM fuel cell is at steady state and at constant temperature and pressure. Both the air and hydrogen are assumed to distribute uniformly and to flow in the laminar regime. The hydrogen and air velocities in the experiment were 4 m s^{-1} and 8 m s^{-1} and their Reynolds numbers were 785 and 1570, respectively. The flow regimes in both cases were close to the transition region but still within the laminar regime. The flow is also assumed to be fully developed everywhere and the velocity is assumed constant. The pressure drops in both cases were quite small at about 440 Pa and 880 Pa, respectively because the friction factors in both cases were low at 0.01 and 0.012, respectively. If hydrogen depletion is ignored, the velocity would only drop slightly and the constant velocity assumption holds. The hydrogen stoichiometric ratio was about 10 and hydrogen usage is only about 10%. Hence if hydrogen depletion was considered, the velocity would only drop by 10% of its inlet value. The velocity can still be assumed constant. The gas mixtures are assumed to behave as an ideal gas. In order to avoid confusion with liquid water, the term moisture is used to denote water vapour in the gases and in the membrane. Since the water management strategy for flood prevention is by keeping the moisture contents of both gases below saturation, the water transport in the gas flow channel is therefore assumed to occur in the gas phase only. The single phase gas flow in the channel can be maintained if the gas velocity is kept quite high even when the moisture in the gas reaches the dew point [53]. The moisture balance in an infinitesimal section of the flow channel of width w, depth b and length dz at the anode as shown in Fig. 1, assuming there is no axial diffusion, is given by:

$$\frac{dy_A}{dz} = \frac{RT}{vbp} J_A \tag{1}$$

where y_A is the molar moisture content in the bulk hydrogen, J_A is the condensation flux of water on the surface of the anode, R is the gas constant, T is the temperature, v is the gas velocity, b is the depth of the flow channel and p is the total gas pressure. The driving force of the moisture mass transfer flux from the hydrogen gas to the membrane by evaporation is given by the difference between y_A and the equilibrium moisture content of the hydrogen feed at the surface of the anode and the anode temperature, y_A^*. As the moisture content of the membrane is low, it is given by Henry's law, $y_A^* = Hx_A^*$, where x_A^* is the equilibrium moisture content of the membrane [54]. If water is assumed to condense on the wet surface

of the anode, then the condensation flux is given by the following relationship for mass transfer:

$$J_A = k_A(y_A - y_A^*) \tag{2}$$

where k_A is the condensation coefficient. Eq. (1) then becomes

$$\frac{dy_A}{dz} = \frac{RTk_A}{vbp}(y_A - y_A^*) \tag{3}$$

The analytical solution is given by

$$y_A = y_A^* + \left(y_{AF} - y_A^*\right)\exp\left(\frac{-z^*}{Pe}\right) \tag{4}$$

where $Pe = vbP/RTk_A$ is the anode Peclet number, $z^* = z/L$ is the dimensionless distance, L is the total length of the flow field and y_{AF} is the hydrogen feed moisture content. The membrane surface on the anode side is assumed to be saturated with water, but the water content at the membrane surface on the cathode side is x_{Ci}, which is not in equilibrium with air. If x_{Ci} is smaller than x_A^*, then there is no back diffusion. At steady state, the water content in the membrane is assumed to drop linearly from the anode to the cathode. This is a reasonable assumption because the fuel cell was run at low current density in such a way as to remove water formed by reaction at the cathode as soon as it was formed by rapid evaporation using low humidity or dry air. The very little accumulation of water on the cathode side was not sufficient to increase its concentration at the cathode side of the membrane to cause any significant back diffusion to the anode. In addition there was a net flow of water from the anode and cathode. The latest study on electro-osmotic drag for PEM fuel cells operated at high hydrogen humidity and dry air [55] which is similar to the present study, confirmed that the moisture content dropped across the membrane from the anode to the cathode and the moisture profile was linear at low current density. Hence, the moisture at the surface of the cathode is given by:

$$x_{Ci} = x_A^* - M = \frac{y_A^*}{H - M} \tag{5}$$

where M is a coefficient. The driving force of the moisture mass transfer flux from the membrane at the cathode is given by the difference in the moisture content at the surface of the cathode and the moisture content in the bulk air, y_A. Hence, the moisture balance in an infinitesimal section of the flow channel of width w, depth b and length dz at the cathode as shown in Fig. 1, assuming there is no axial diffusion, is given by:

$$\frac{dy_C}{dz} = \frac{RT}{vbP}(J_C + r) \tag{6}$$

where J_C is the condensation flux of water on the surface of the anode and r is the rate of water produced by the electrochemical reaction at the cathode per unit area of cathode. If water is assumed

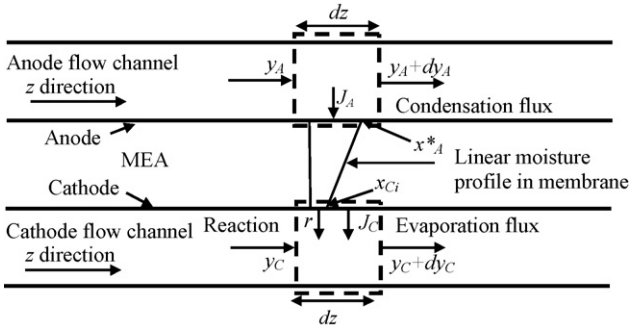

Fig. 1. Schematic diagram of control volumes for differential mass balance of water in the anode and cathode gas channels in a PEM fuel cells.

to evaporate from the wet surface of the cathode, then the evaporation flux from the wet surface of the cathode is given by the following [56,57]:

$$J_C = k_C(y_{Ci} - y_C)^n \tag{7}$$

where y_{Ci} is the water content of the air near the surface of the cathode, which is assumed to approximate Raoult's Law at the cathode's surface. By virtue of Eq. (5), y_{Ci} is given by:

$$y_{Ci} = Kx_{Ci} = K\left(\frac{y_A^*}{H - M}\right) \tag{8}$$

where K is a coefficient and k_C is the evaporation mass transfer coefficient, given by:

$$k_C = D + Ev^m \tag{9}$$

The values of n and m are either 1.0 and 0.5756, respectively, for the Bansal and Xie evaporation model [56] or 0.82 and 1.0, respectively, for the Tang and Etzion evaporation model [57]. The rate of water produced by the electrochemical reaction, r, at the cathode is given by:

$$r = \frac{i_c}{2F} \tag{10}$$

After simplifying the current density expression, i_C, [58] it can be written as:

$$i_C = \frac{p}{RT}G(1 - y_C) \tag{11}$$

where:

$$G = K_4(1 - \sqrt{K_5\exp(-K_6(\phi_s - \phi_m - \phi_{eq}^c)}))) \times \coth\sqrt{K_5\exp(-K_6(\phi_s - \phi_m - \phi_{eq}^c))} \tag{12}$$

$$K_4 = \frac{24t_e(1-\varepsilon)FD_{O_2}}{d_p^2} \tag{13}$$

$$K_5 = \frac{i_{OC}a_s d_p^2}{16FC_{O_2}^{ref}D_{O_2}} \tag{14}$$

$$K_6 = \frac{F}{2RT} \tag{15}$$

where t_e is thickness of the *GDL*, d_p is the pore diameter, ε is the dry porosity, a_s is the specific active surface area, $C_{O_2}^{ref}$ is the reference molar concentration of oxygen, ϕ_s and ϕ_m are electrode and membrane potentials, respectively, $\Delta\phi_{eq}$ is the potential difference between the electrode and the membrane, F is the Faraday's constant, D_{O_2} is the diffusion coefficient of the dissolved oxygen in the electrolyte and i_{OC} is the cathodic exchange current density. Eq. (6) can be rewritten as:

$$\frac{dy_C}{dt} = \frac{RTk_C}{vbP}\left(K\left(\frac{y_A^*}{H - M}\right) - y_C\right)^n + \frac{G}{2Fvb}(1 - y_C) \tag{16}$$

$$\frac{dy_C}{dz^*} = \frac{1}{Pe}(Q - y_C)^n + \frac{Da}{Pe}(1 - y_C) \tag{17}$$

where $Pe = vbP/RTk_C$ is the cathode Peclet number, $Da = G/2Fk_C$ is the Damkohler number and $Q = K\left(y_A^*/H - m\right)$. If m is small and $K \approx H$, then $Q \approx y_A^*$. If n and m are not integers, then Eq. (17) has no closed form analytical solution and can only be solved by using a numerical method such as the fourth order Runge Kutta algorithm. However, if the adopted values n and m are 1.0 and 0.5756 [56], respectively, and if the velocity is relatively constant throughout the channel, then Eq. (17) becomes:

$$\frac{dy_C}{dz^*} = \frac{Da + Q}{Pe} - \left(\frac{Da + 1}{Pe}\right)y_C \tag{18}$$

If Eq. (20) is integrated with respect to y_C, then:

$$y_C = \frac{(Da + Q)}{(Da + 1)} + \left[y_{CF} - \frac{(Da + Q)}{(Da + 1)}\right] \exp\left[-\left(\frac{Da + 1}{Pe}\right) z^*\right] \quad (19)$$

Since the relative humidity, ϕ, is the parameter that is measured in the experiment, a relationship between the mole fraction and the relative humidity is needed. The mole fraction of water vapour is given by:

$$y = \phi \frac{p_{sat}}{p} \quad (20)$$

where p_{sat} is the saturated vapour pressure of water. The moisture flux across the membrane, J_w, can also be written in terms of the overall gas side mass transfer coefficient, k_g:

$$J_w = k_g (y_a - y_c) \quad (21)$$

The overall gas side moisture mass transfer coefficient k_g for both the anode and cathode can be estimated from the anode and the cathode moisture mass transfer coefficients k_A and k_C:

$$\frac{1}{k_g} = \frac{K}{k_A} + \frac{1}{k_C} \quad (22)$$

Both Eqs. (4) and (19) were to be validated by experimental data from a single cell PEMFC that was run at different temperatures. An alternative water management strategy that forces the water to flow from the anode to the cathode was implemented in the experiment. This was achieved by saturating the hydrogen feed ($\phi = 1$) and using dry air ($\phi = 0.005$). Two pressure levels were used, 1 bar and 1.5 bar at the anode and the cathode, respectively.

4. Materials and methods

4.1. Single cell PEMFC

A single cell PEMFC was fabricated and used for the model validation. The specifications of the single cell PEMFC are given Table 1. Fig. 2 shows the graphite plate with a conventional serpentine flow field and the positions of the three humidity sensors installed along the field. The positions of the humidity sensors on the anode and cathode are shown in Fig. 3. An expanded view showing the various components of the single cell is shown in Fig. 4. Two humidity sensors were also installed at the feed points of the air and hydrogen on the single cell to measure the external humidity of reactant gas before entering the cell.

The temperature of the single cell fuel cell was controlled by temperature controllers in the Fuel Cell Test Station for both hydrogen and air flows. The humidity sensors were read when a steady state of operation was established after 2 h of operation. A schematic flow diagram of the experimental setup is shown in Fig. 5.

Table 1
Single cell PEM fuel cell specifications.

Size	200 mm × 200 mm × 5 mm
Active area	200 cm^2
Active layer thickness	5 μm
Specific surface area	1.0×10^7 m^2 m^{-3}
Flow field pattern	Serpentine
Flow channel	Gas channel size: width = 5 mm, depth = 2.5 mm, Rib = 2.5 mm, length = 2989 mm
Current collector	Copper
End plate	Aluminium = 0.01 m
Gasket	Silicone rubber 0.001 m
Electrolyte membrane	Nafion® 112
Position of humidity sensor 1	457 mm
Position of humidity sensor 2	1266 mm
Position of humidity sensor 3	2532 mm

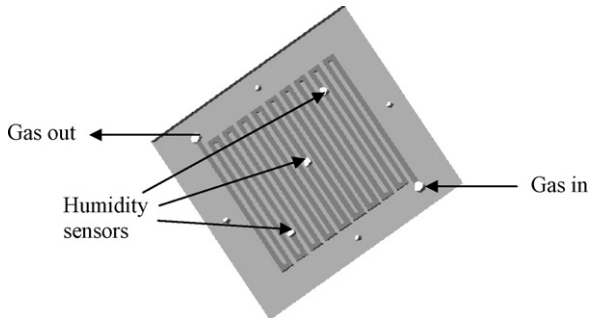

Fig. 2. Serpentine flow field with three holes for the humidity sensors.

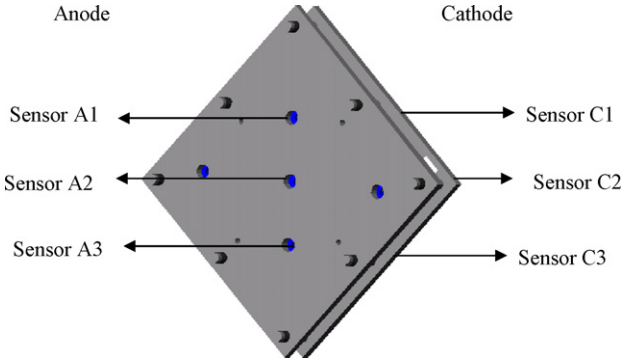

Fig. 3. Position of humidity sensors on both the anode and cathode.

4.2. Experimental work

An Arbin Fuel Cell Test Station was used to test the single cell PEMFC. The temperature was varied from 25 °C to 60 °C, while the pressure at the anode and the cathode was kept at 1 bar and 1.5 bar, respectively. The flow rates of hydrogen and air were fixed at 3 L min^{-1} and 6 L min^{-1}, respectively. The high flow rates were chosen so that single phase gas flow in the channel was ensured even when the moisture in the gas reaches saturation [53]. Table 2 shows the operational parameters of the cell. The single cell fuel cell was operated by externally humidifying the hydrogen feed gas at the anode until it was saturated with moisture ($\phi = 1.0$). The air at the cathode was dried to a low relative humidity, $\phi = 0.005$. The water profile models at the anode and the cathode were then validated by the humidity profiles along the serpentine flow field. The polarization curves for the single cell PEMFC during the experiment at various temperatures are shown in Fig. 6.

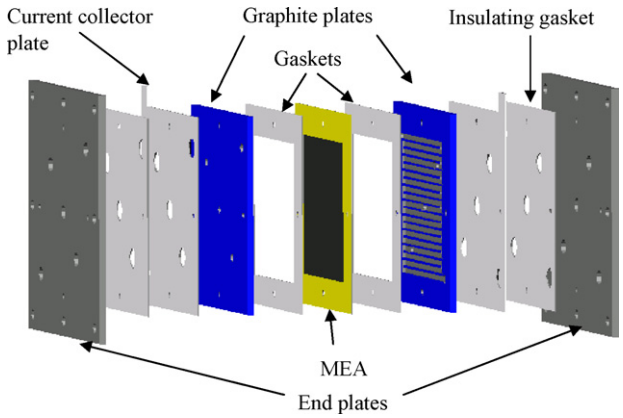

Fig. 4. Expanded view of the single cell PEMFC.

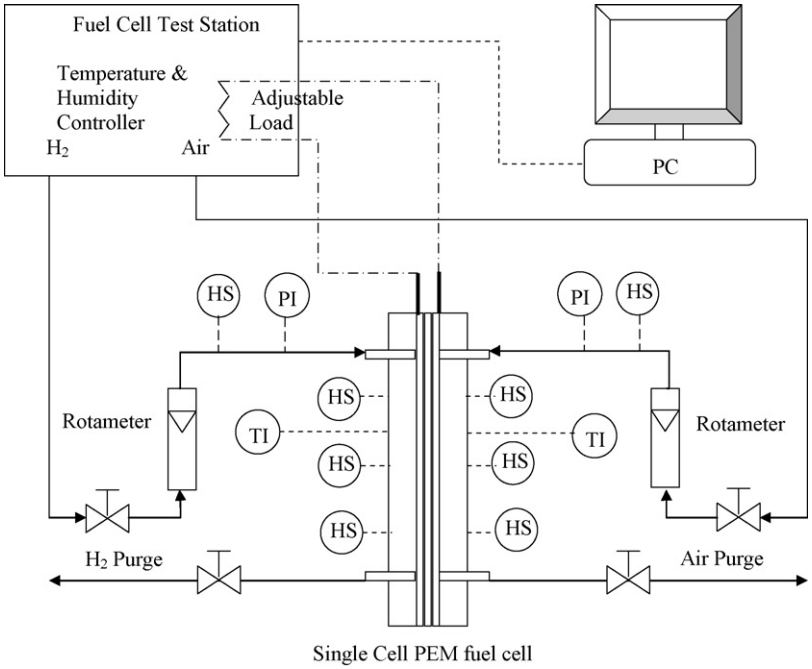

Fig. 5. Schematic diagram of experimental setup.

Table 2
Operating parameters of single cell PEM fuel cell.

Operating parameters	Value
Cell pressure	1.0–1.5 bar
Cell temperature	25–60 °C
Hydrogen flow rate	3 L min^{-1}
Air flow rate	6 L min^{-1}
Relative humidity (anode)	1.0 RH
Relative humidity (cathode)	0–0.005 RH
Exchange current density	10 mA cm^{-2}
The potential of electrode	0.6–0.8 V

5. Results and discussion

Fig. 7 shows the four-point moisture content profiles at four different temperatures along the serpentine flow field on the anode side that were measured when a steady state was reached after 2 h of operation. Since the hydrogen feed was saturated with moisture, its moisture content increased with temperature. The moisture content profile of the hydrogen decreased more rapidly as temperature was increased because the mass flux rate of moisture through the MEA increased more dramatically with increasing temperature.

The similarly obtained moisture content profiles on the cathode side are shown in Fig. 8. The moisture content profiles increased more rapidly at a higher temperature because the mass flux rate of moisture through the MEA and the rate of water production by the electrochemical reaction at the cathode increased more drastically with increasing temperature.

The model equations were validated by determining their parameters on the anode and cathode sides using the least squares algorithm. The experimentally determined parameters are given in Tables 3 and 4. The sums of squares of residuals are all very small, indicating that all the experimental data closely fit the model equations. These results show that the use of the water evaporation model of Bansal and Xie [56] in the moisture profile model leads to a simple closed form solution that was easily fitted to the experimental data. The evaporation model of Tang and Etzion [57] did

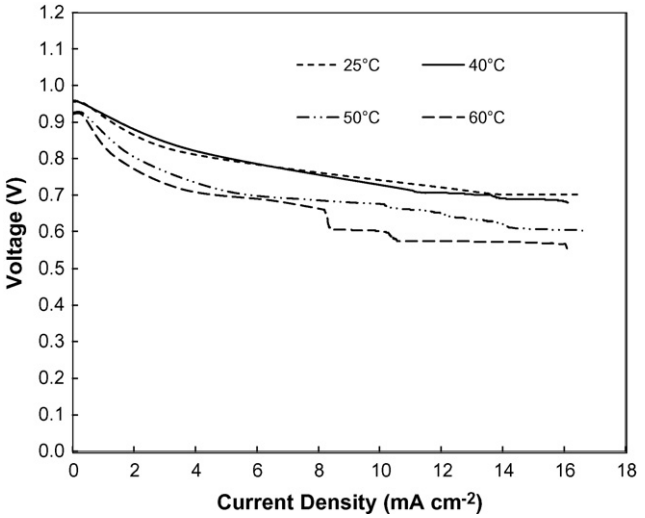

Fig. 6. Polarization curves of the MEA at constant temperatures.

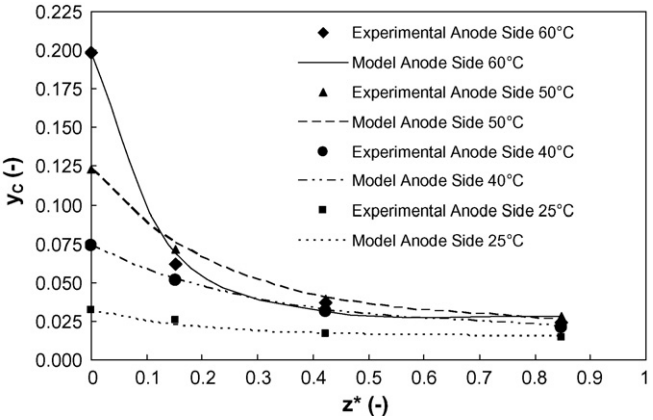

Fig. 7. Moisture content profiles on the anode side at various temperatures.

Table 3
Parameter estimation of the model equation on the anode side.

Temperature (°C)	y_{AF}	y^*_A	1/Pe	Pe	Sum of squares of residuals
25	0.03223	0.01503	0.01702	58.7544	7.3×10^{-6}
40	0.07405	0.01798	1.10600	0.9042	3.0×10^{-7}
50	0.12330	0.02301	1.41020	0.7091	2.3×10^{-6}
60	0.19880	0.02810	3.10500	0.3221	9.8×10^{-6}

Table 4
Parameter estimation of model equation on the cathode side.

Temperature (°C)	y_{CF}	$(Da + y^*_A)/(Da + 1)$	$(Da + 1)/Pe$	Pe	Da	Sum of squares of residuals
25	0.000203	0.01702	0.00901	111.210	0.00202	9.1×10^{-7}
40	0.000396	0.02801	1.15010	0.878	0.01021	9.6×10^{-6}
50	0.000621	0.03210	1.20001	0.841	0.00930	5.6×10^{-6}
60	0.000751	0.02705	1.20102	0.831	0.00010	1.6×10^{-6}

not lead to a closed form solution and was therefore not pursued further in this paper.

The moisture profiles on the anode side were influenced by the Peclet number, which compares the relative strengths of convection and mass transfer processes. The large value of the Peclet number at 25 °C compared to that at higher temperatures indicated that the mass flux is very small compared to the convection of the gas at this temperature. The Peclet number on the anode side decreased from 59 to 0.32 when temperature was increased from 25 °C to 60 °C. This was caused not only by the increasing moisture mass transfer coefficient and moisture diffusion in the membrane with temperature, but also by water molecules being dragged by the proton stream across the membrane by electro-osmotic drag.

On the other hand, the moisture profiles on the cathode side were influenced by both the Peclet and the Damkohler numbers. The Damkohler number compares the relative strengths of the electrochemical reaction and mass transfer processes at the cathode. The Peclet number on the cathode side shows a similar trend to the Peclet number on the anode side. However, the Damkohler number initially increased to a maximum at 40 °C, but then fell back to a lower level at 60 °C. It can be deduced that the removal rate of moisture by mass transfer was initially outstripped by moisture production from the electrochemical reaction up to 40 °C. Above 40 °C the moisture removal rate by mass transfer overtook the rate of moisture production from the electrochemical reaction at higher temperatures up to 60 °C.

Figs. 9–12 show the composite moisture profiles at both the anode and the cathode at various temperatures. The moisture gradient across the MEA was initially large because the hydrogen feed was saturated with moisture and the air was dry. Both the anode and the cathode moisture profiles converged to the same asymptotic value for each temperature. The asymptotic moisture content values correspond to the equilibrium moisture contents of the membrane at the same temperature.

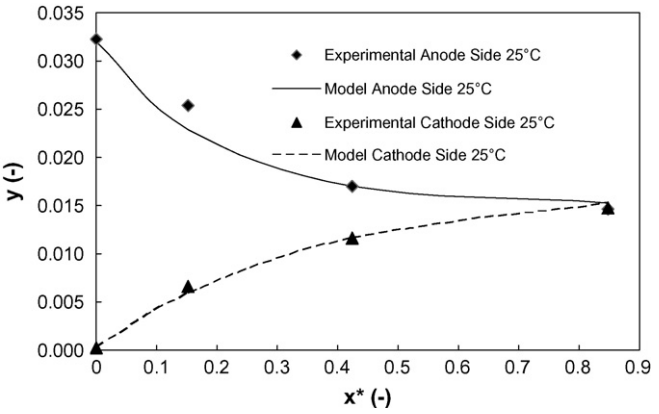

Fig. 9. Moisture content profiles in the anode and cathode at 25 °C.

The anode moisture mass transfer coefficient, k_A, cathode moisture mass transfer coefficient, k_C, and overall moisture mass transfer coefficient, k_g, were estimated from the Peclet number data and are shown in Table 5. Moisture fluxes across the MEA at various temperatures are shown in Fig. 13.

The overall moisture mass transfer coefficients and the effective moisture diffusivities are of the same order of magnitude as those given in a previous work [59], except at 25 °C. The large discrepancy at 25 °C is caused by the loss of accuracy of the humidity measurement at low temperature. The order of magnitude correspondence

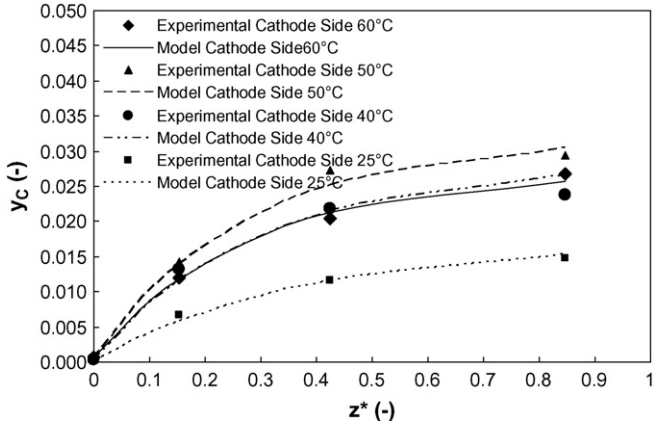

Fig. 8. Moisture content profiles on the cathode side at various temperatures.

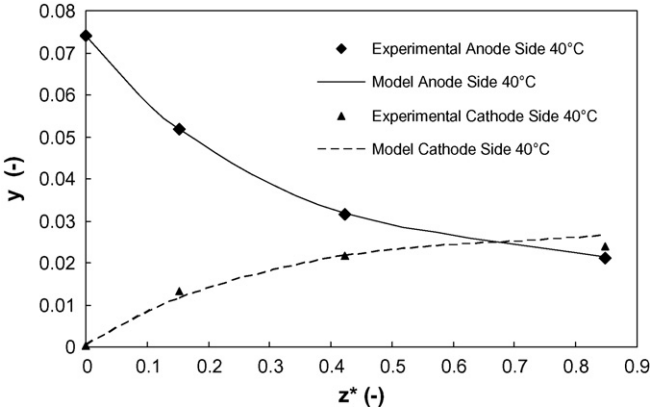

Fig. 10. Moisture content profiles in the anode and cathode at 40 °C.

Table 5
Estimated values of moisture mass transfer coefficient and effective diffusivity.

k_A (mol cm^{-2} s^{-1})	k_C (mol cm^{-2} s^{-1})	K-values for moisture [16]	Experimental k_g (mol cm^{-2} s^{-1})	Published k_g (mol cm^{-2} s^{-1}) [22]	Experimental D_E (mol cm^{-2} s^{-1})
4.66×10^{-5}	2.46×10^{-5}	54.93	8.19×10^{-7}	1.35×10^{-5}	1.64×10^{-8}
2.88×10^{-3}	2.97×10^{-3}	64.43	4.41×10^{-5}	2.85×10^{-5}	8.81×10^{-7}
3.56×10^{-3}	3.00×10^{-3}	70.75	4.95×10^{-5}	3.60×10^{-5}	9.99×10^{-7}
7.60×10^{-3}	2.94×10^{-3}	77.08	9.54×10^{-5}	4.70×10^{-5}	1.91×10^{-6}

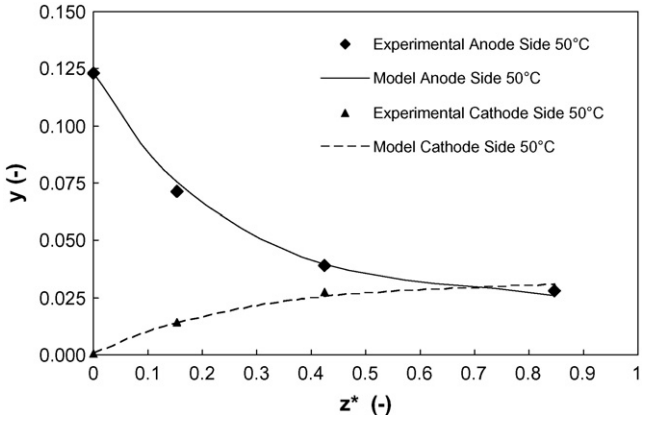

Fig. 11. Moisture content profiles in the anode and cathode at 50 °C.

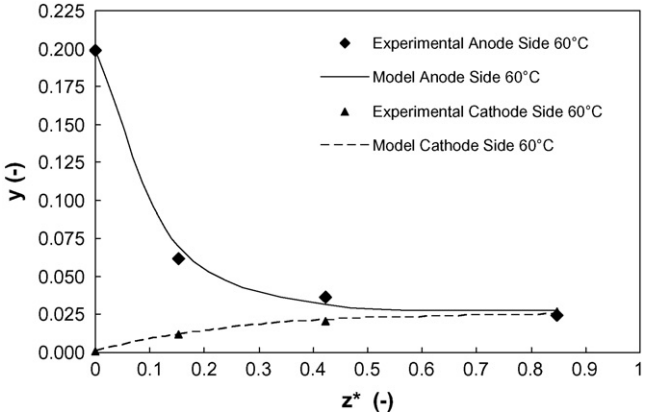

Fig. 12. Moisture content profiles in the anode and cathode at 60 °C.

of the overall mass transfer coefficients and the effective moisture diffusivities with published data validates the model.

Moisture flux increased with increasing temperature, but decreased along the flow field and vanished at the outlet of the flow field when the moisture content reached the equilibrium moisture content of the membrane at the outlet. Water formed by the reaction and moisture from the anode was immediately removed by the dry air because of the large moisture content gradient between the cathode and the dry air. The moisture did not reach its dew point at any point in the cathode, and no water droplets that may have caused flooding were formed in the cathode. The conventional strategy of saturating both the hydrogen and air feeds was found to cause rapid formation of water droplets in the cathode side, flooding and blocking the flow field channels [60] and the electrode [61], because moisture dew point was already reached near the air inlet [61].

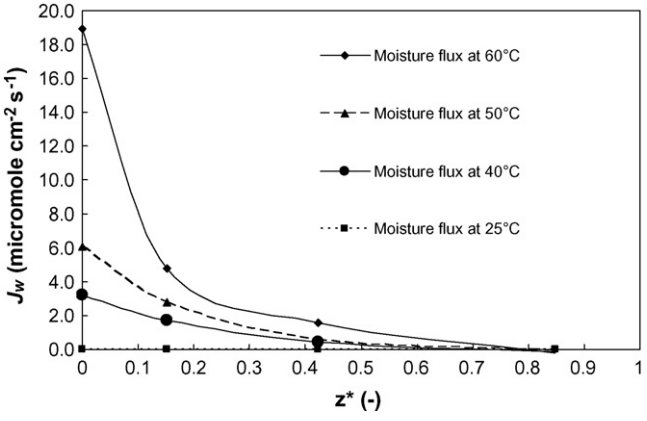

Fig. 13. Moisture flux across the MEA at various temperatures.

6. Conclusions

The moisture profile in the flow field channels of the anode was shown to depend on the moisture Peclet number, the decrease of which with increasing temperature indicates increasing moisture mass transfer. On the other hand, the moisture profile in the cathode was shown to depend on both the Peclet number and the Damkohler number. The trend of the Peclet number in the cathode followed closely that of the anode. The Damkohler number decreased with temperature, indicating increasing moisture mass transfer. The moisture profile models were successfully validated by the published data of the estimated overall mass transfer coefficient and moisture effective diffusivity with those in published data of the same order of magnitude. The strategy of saturating the hydrogen feed and using dry air in the present work has been shown to successfully prevent water droplet formation in the cathode and hence prevent flooding.

Acknowledgements

The authors would like to thank the Malaysian Ministry of Science, Technology & Innovation for sponsoring this work under project IRPA 02-02-02-0001-PR0023/11-06.

References

[1] F. Buchi, S. Srinivasan, J. Electrochem. Soc. 144 (1997) 2767–2772.
[2] K.H. Choi, D.J. Park, Y.W. Rho, Y.T. Kho, T.H. Lee, J. Power Sources 74 (1998) 146–150.
[3] D. Hyun, J. Kim, J. Power Sources 126 (2004) 98–103.
[4] S.E. Iyuke, A.B. Mohamad, W.R.W. Daud, Chem. Eng. Sci. 56 (2001) 4949–4956.
[5] T.E. Springer, T.A. Zawodzinski, S. Gottesfeld, J. Electrochem. Soc. 138 (8) (1991) 2334–2341.
[6] T.V. Nguyen, R.E. White, J. Electrochem. Soc. 140 (8) (1993) 2178–2186.
[7] J.S. Yi, T.V. Nguyen, J. Electrochem. Soc. 145 (4) (1998) 1149–1159.
[8] P. Sridhar, R. Perumal, N. Rajalakshmi, M. Raja, K.S. Dhathathreyan, J. Power Sources 101 (1) (2001) 72–78.
[9] R. Mosdale, G. Gebel, M. Pineri, J. Membr. Sci. 118 (1996) 269–277.
[10] F. Chen, H-S. Chu, C.Y. Soong, W.-M Yan, J. Power Sources 140 (2005) 243–249.
[11] J. Zhang, Y. Tang, C. Song, X. Cheng, J. Zhang, H. Wang, Electrochim. Acta 52 (2007) 5095–5101.
[12] M.G. Santarelli, M.F. Torchio, Energy Convers. Manage. 48 (2007) 40–51.
[13] F.N. Buchi, A.B. Geiger, R.P. Neto, J. Power Sources 145 (2005) 62–67.
[14] D.M. Bernardi, M.W. Verbrugge, J. Electrochem. Soc. 139 (9) (1992) 2477–2491.
[15] F. Gloaguen, R. Durand, J. Appl. Electrochem. 27 (1997) 1029–1035.
[16] K. Weisbrod, S. Grot, N. Vanderborgh, Proceedings of the first international symposium on proton conduction membrane fuel cells, vol. I, 1995, pp. 153–166.
[17] C. Marr, X. Li, ARI 50 (1998) 190–200.

[18] J. Baschuk, X. Li, J. Power Sources 86 (2000) 181–196.
[19] L. Pisani, G. Murgia, M. Valentini, B. D'Aguanno, J. Electrochem. Soc. 149 (2002) A898–A904.
[20] T.F. Fuller, J. Newman, J. Electrochem. Soc. 140 (5) (1993) 1218–1224.
[21] D. Natarajan, T. Nguyen, J. Power Sources 115 (2003) 66–80.
[22] G. Inoue, Y. Matsukuma, M. Minemoto, J. Power Sources 154 (2006) 8–17.
[23] S. Shimpalee, S. Dutta, W. Lee, J. Van Zee, Am. Soc. Mech. Eng., Heat Transfer Div. 364 (1999) 367–374.
[24] S. Shimpalee, S. Dutta, J. Van Zee, Am. Soc. Mech. Eng., Heat Transfer Div. 366 (2000) 1–9.
[25] T. Berning, D. Lu, N. Djilali, J. Power Sources 106 (2002) 284–294.
[26] M. Martinez, S. Shimpalee, J. Van Zee, Comparison of Maxwell–Stefan and CFD and approximation equations for PEMFC applications. Proton exchange membrane fuel cells, vol. V, The Electrochemical Society, Los Angeles, USA, October 16–21, 2005.
[27] S. Shimpalee, W. Lee, J. Van Zee, H. Naseri-Neshat, J. Power Sources 156 (2006) 355–368.
[28] A. Kulikovsky, J. Electrochem. Soc. 150 (2004) A1432–A1439.
[29] Z. Liu, Z. Mao, C. Wang, J. Power Sources 158 (2006) 1229–1239.
[30] M. Khakbaz Baboli, M.J. Kermani, Electrochim. Acta 53 (2008) 7644–7654.
[31] A.D. Le, B. Zhou, J. Power Sources 182 (2008) 197–222.
[32] V. Gurau, H. Liu, S. Kakac, AIChE J. 44 (1998) 2410–2422.
[33] J. Baschuk, X. Li, J. Power Sources 142 (2005) 134–153.
[34] J. Baschuk, X. Li, Appl. Energy 86 (2009) 181–193.
[35] C. Wang, Z. Wang, Y. Pan, Am. Soc. Mech. Eng., Heat Transfer Div. 364 (1999) 351–357.
[36] S. Um, C. Wang, K. Chen, J. Electrochem. Soc. 147 (2000) 4485–4493.
[37] S. Um, C. Wang, J. Power Sources 156 (2006) 211–223.
[38] Y. Wang, C. Wang, K. Chen, Electrochim. Acta 52 (2007) 3965–3975.
[39] N.P. Siegel, M.W. Ellis, D.J. Nelson, M.R. Spakovsky, J. Power Sources 128 (2) (2003) 173–184.
[40] V. Gurau, T. Zawodzinski, J. Mann, Numerical investigation of water transport in the PEMFC components. Proton exchange membrane fuel cells, vol.6, The Electrochemical Society, Cancun, Mexico, October 29–November 3, 2006.
[41] H. Meng, C. Wang, J. Electrochem. Soc. 152 (2005) A1733–A1741.
[42] M. Coppo, N. Siegel, M. von Spakovsky, J. Power Sources 159 (2006) 560–569.
[43] G. He, P. Ming, Z. Zhao, A. Abudula, Y. Xiao, J. Power Sources 163 (2007) 864–873.
[44] L. Yu, G. Ren, M. Qin, X. Jiang, Renewable Energy 34 (2009) 530–543.
[45] J.C. Amphlett, R.F. Mann, B.A. Peppley, P.R. Roberge, A. Rodrigues, J. Power Sources 61 (1996) 183–188.
[46] J.T. Pukrushpan, A.G. Stefanopoulou, H. Peng, IEEE Control Syst. Mag. 24 (2004) 30–46.
[47] Y. Shan, S.Y. Choe, J. Power Sources 145 (2005) 30–39.
[48] J. Benziger, E. Chia, E. Karnas, J. Moxley, C. Teuscher, I.G. Kevrekidis, AIChE J. 50 (8) (2004) 1889–1900.
[49] J.R. Kolodziej, J. Fuel Cell Sci. Technol. 4 (3) (2007) 255–260.
[50] E.-S.J. Chia, J.B. Benziger, I.G. Kevrekidis, AIChE J. 52 (11) (2006) 3902–3910.
[51] Y.-S. Chen, H. Peng, J. Power Sources 185 (2008) 1179–1192.
[52] H. Huisseune, A. Willockx, M. De Paepe, Int. J. Hydrogen Energy 33 (2008) 6270–6280.
[53] L. Zhang, H.T. Bi, D.P. Wilkinson, J. Stumper, H. Wang, J. Power Sources 183 (2008) 643–650.
[54] M. Legras, Y. Hirata, Q.T. Nguyen, D. Langevin, M. Metayer, Desalination 147 (2002) 351–357.
[55] Y.H. Park, J.A. Caton, Int. J. Hydrogen Energy 33 (2008) 7513–7520.
[56] P.K. Bansal, G. Xie, Int. Comm. Heat Mass Transfer 25 (2) (1998) 183–190.
[57] R. Tang, Y. Etzion, Building Environ. 39 (2004) 77–86.
[58] M. Grujicic, K.M. Chittajallu, Appl. Surf. Sci. 227 (2004) 56–72.
[59] P.W. Majsztrik, M.B. Satterfield, A.B. Bocarsly, J.B. Benziger, J. Membr. Sci. 301 (2007) 93–106.
[60] A.L. Ballard, E.D. Sloan Jr., Fluid Phase Equilib. 218 (2004) 15–31.
[61] Z.W. Dunbar, R.I. Masel, J. Power Sources 182 (2008) 76–82.